THE JOURNAL OF PHYSICAL CHEMISTRY C

Article

pubs.acs.org/JPCC

Reducing the Matrix Effect in Molecular Secondary Ion Mass Spectrometry by Laser Post-Ionization

Lars Breuer,*[,†] Nicholas J. Popczun,[†] Andreas Wucher,[‡] and Nicholas Winograd[†]

[†]Department of Chemistry, The Pennsylvania State University, 104 Chemistry Building, University Park, Pennsylvania 16802, United States

[‡]Fakultät für Physik, Universität Duisburg-Essen, 47048 Duisburg, Germany

Supporting Information

ABSTRACT: Strategies to reduce and overcome matrix effects in molecular secondary ion mass spectrometry (SIMS) are investigated using laser-based post-ionization of sputtered neutral organic molecules released under C_{60}^+ bombardment. Using a two-component multilayer film similar to that employed in a recent VAMAS interlaboratory study, SIMS depth profiles of the protonated and deprotonated quasi-molecular ions of two well-studied organic molecules, Irganox 1010 and Irganox 1098, were measured along with that of the corresponding neutral precursor molecules. When compared to composition-dependent ionization probability changes of the secondary ions, the resulting profiles are much improved. We demonstrate that detection of neutral molecules via laser post-ionization yields significantly reduced matrix effects when compared to SIMS depth profiles in both positive and negative secondary ion mode. These results suggest that this approach may provide a useful pathway for acquiring depth profiles from complex organic samples with improved capabilities for quantitation.

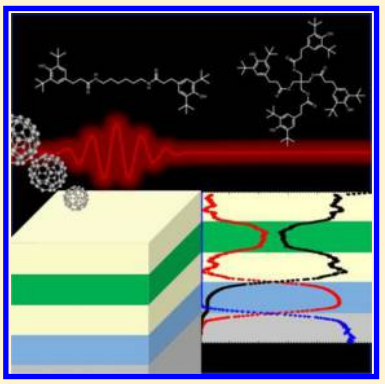

INTRODUCTION

Cluster secondary ion mass spectrometry (SIMS) has emerged as a unique tool for the two- and three-dimensional (2D/3D) characterization of complex organic materials, including biological cells.[1−3] The critical breakthrough for this technology is the discovery that by employing primary ion beams such as Bi_3^+, C_{60}, or Ar_n, with n = 500−5000, mass spectra can be acquired during erosion of the sample without undue chemical damage accumulation.[4,5] Moreover, since the beams are focusable to a submicron spot, high-resolution chemical imaging has become a major distinguishing feature of the technique. In concert with the development of these primary ion sources, there have also been rapid advances in instrumentation that seeks to maximize the properties associated with the desorption events. These improvements have immensely expanded the number and type of applications amenable for study.

All of this good news for cluster SIMS is still tempered by the fact that the ionization probability of the desorbing molecules is discouragingly small for most cases, limiting sensitivity.[6,7] Moreover, these probabilities are subject to enormous swings in value depending upon the chemical composition of the sample. Matrix ionization effects render quantification of intensities very difficult, because they are not easily predictable or controllable.[8]

As these issues are still a major problem for the technique, many groups have concentrated on acquiring a better understanding of matrix ionization effects, and on developing protocols for enhancing the ionization probability itself. A landmark (VAMAS) study was recently completed using a standard reference material consisting of layers of binary mixtures of Irganox 1010, Irganox 1098, or Fmoc-pentafluoro-L-phenylalanine in each layer.[9] Twenty different laboratories characterized the sample, yielding results of remarkable consistency. Recommendations were provided for compensating for matrix effects, and a normalization method was presented that greatly improves quantitation. Other groups have attempted to enhance the ionization probability either by modifying the chemistry of the sample to allow for better protonation of desorbing molecules or by tweaking the chemistry of the incoming cluster ion beam. For example, gas cluster ion sources consisting of water clusters have been employed to enhance ionization via protons carried by the projectile.[10,11] Alternatively, we have advocated doping the gas clusters with reactive species such as HCl in combination with depositing water directly onto the surface of the sample to provide a source of protons in a protocol characterized by dynamic reactive ionization (DRI).[12,13]

Another approach to mitigating matrix effects and enhancing ionization is to employ laser techniques to ionize the neutral molecules after they have desorbed from the surface.[14] Laser post-ionization (LPI) has been utilized for many years with mixed success. Problems arise because the laser is observed to fragment molecules during the ionization process, and in many cases the improvement of signal intensity over direct detection of secondary ions is modest. The concept is still intriguing, however, because changes in the number of molecules entering

Received: March 19, 2017
Revised: May 20, 2017
Published: July 7, 2017

DOI: 10.1021/acs.jpcc.7b02596
J. Phys. Chem. C 2017, 121, 19705−19715

the ionization channel via SIMS do not influence the number of sputtered neutral molecules, except for the rare cases where ionization efficiency approaches 100%. Recently, we have reported that femtosecond-pulsed lasers operating in the strong field regime and in the IR spectrum greatly reduce photofragmentation and result in excellent sensitivity for a wide range of molecules.[15,16]

Here, we take advantage of this laser configuration to employ LPI to characterize a binary mixture of multilayers of Irganox 1010 and Irganox 1098 similar to that investigated in the VAMAS study to examine the magnitude of matrix effects associated with the neutral desorption channel. With a primary ion beam of 20 keV C_{60}, the results show that matrix effects are effectively overcome during molecular depth profiling and that the molecular ion intensity of Irganox is comparable to that observed using SIMS. In general, we suggest that this approach may provide a useful pathway for acquiring depth profiles from complex organic samples with improved capabilities for quantitation.

EXPERIMENTAL SECTION

Experimental Setup. The experiments presented here were performed on a time-of-flight sputtered neutral mass spectrometer (SNMS) instrument described in great detail elsewhere.[17] In brief, the systems consists of a 40 keV C_{60}^+ ion source delivering an ion current on about 200 pA into a spot of about 10 μm diameter, a temperature-controlled sample stage, a reflectron type mass-spectrometer, a movable focusing lens and a laser utilized for post-ionization.

For post-ionization, a commercially available laser system (Coherent, Legend Elite Duo) was used. This system delivers short laser pulses with a wavelength of 800 nm and a duration of 40 fs at a repetition rate of 1 kHz. These laser pulses are used to pump an optical parametric amplifier (OPA, Light Conversion, TOPAS-C-HE) to shift the light further into the IR covering a range from 1160 to 2580 nm. For the experiments presented in this work, a wavelength of 1500 nm and an average power of 1.9 W was selected. From previous experiments[18,19] it is known that for the intact ionization of organic molecules the wavelength should be chosen as far as possible into the NIR regime. The selected wavelength of 1500 nm gives the benefit of a longer wavelength while still maintaining significant power density.

The laser beam is coupled into the system and focused by a BK7 lens with a focal length of 150 mm at a wavelength of 587.6 nm. The lens is mounted onto an *x,y,z* translation stage to optimize the overlap with the plume of sputtered particles. To achieve maximum LPI signal in the mass spectra, the laser beam is defocused to a volume of about 10 times that of its fully focused position. This defocusing is accomplished by moving the lens along the *z*-axis parallel to the direction of the laser propagation by 6.5 mm with respect to the focal position. The experiment was tuned for SIMS and LPI experiments in the same way to ensure identical conditions. For that purpose, a delayed extraction scheme was used. A relatively long primary ion pulse of 2000 ns was utilized and the sample pulsed to an extraction potential of 2500 V within a few nanoseconds following the end of the primary ion pulse. This extraction technique allows the particles emitted during the primary ion pulse to form a plume above the sample surface, which is then intersected by the post-ionization laser pulse. In SIMS experiments, secondary ions present in the intersection volume that have been emitted from the sample surface during bombardment are extracted into the spectrometer and reflected by a static electrical field of 2507 V at the top of the flight tube toward the detector. In SNMS experiments, the post-ionization laser is fired between the end of the primary ion pulse and the switching of the sample stage to high voltage. In this mode, secondary ions and postionized neutrals present in the intersection volume are detected under otherwise identical experimental conditions with regard to the accepted emission energy and angle window and detection efficiency.

The secondary and postionized ions are detected using a Chevron type microchannel plate (MCP) detector. The output of this detector was fed into a fast 100 times preamplifier and directly digitized using a fast transient recorder (Signatec PX-1500). In addition to photoionized sputtered neutrals, residual gas particles will also be ionized and swept into the spectrometer when in the overlap between the sensitive volume of the spectrometer and the ionization laser. In fact, residual gas neutral molecules represent the majority of detected species in the low mass region that can easily saturate the detector. To avoid deleterious effects from detector gain saturation, the MCP detector is equipped with two highly transmitting grids that can be utilized to deflect these overly abundant ions. The first grid is grounded to avoid any distraction electrical fields in the spectrometer whereas the second grid can be pulsed to a high voltage to reflect ions. Because of the proximity of the grid to the MCP, the ions are already well separated in time and certain regions in the spectrum can be blocked off. In the experiments presented in this study, the low mass region below 200 amu was suppressed by this technique. To increase the signal, especially in the high mass region, a postacceleration voltage of 13 kV was applied to the front of the MCP detector.

Sample Systems. As model systems, Irganox 1010 (Ciba Specialty Chemicals Corporation, U.S.A.) and Irganox 1098 (Aurum Pharmatech Inc., U.S.A.) were investigated. For preliminary studies, pure films of each material were used. Thin films of the materials were spin-cast onto Si wafers from 0.025 M solutions in chloroform (EMD Millipore Corporation, U.S.A.).

Samples containing mixtures of both substances were obtained from the National Physical Laboratory (Teddington, England) from the batch with serial no. SRT14CC. The sample was designed to consist of four different layers on silicon as shown in Figure 1. Each layer was created by physical vapor deposition (PVD) and has a nominal thickness of 100 nm. To create a mixed layer of Irganox 1010 and Irganox 1098, alternating deposition cycles were performed with each cycle depositing only one-half-monolayer coverage of the respective

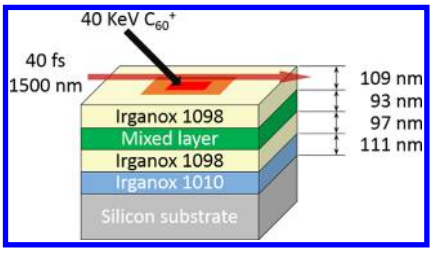

Figure 1. Sample design and sketch of experimental. Multilayer sample, yellow Irganox 1098, blue Irganox 1010, and green mixed layer of Irganox 1098 and Irganox 1010. Black arrow: 40 keV C_{60}^+ beam; red arrow: laser beam parallel to the sample surface. The red square on the sample depicts the analyzed area of 226 × 226 μm^2 and the orange square the sputtered area of 339 × 339 μm^2.

DOI: 10.1021/acs.jpcc.7b02596
J. Phys. Chem. C 2017, 121, 19705−19715

materials.[8] The order of the layers from the top to the silicon substrate is as follows: first a pure Irganox 1098 layer, followed by a mixed layer of Irganox 1010 and Irganox 1098, each with 50% volume fraction (referred to as "concentration" in the remainder of this paper). The mixed layer is followed by another pure Irganox 1098 layer and finally a pure Irganox 1010 layer (Figure 1).

Data Acquisition. Depth profiling of these films was performed with a series of alternating sputter erosion and data acquisition cycles. During data acquisition, the pulsed primary C_{60}^+ ion beam was raster scanned across an area of 226 × 226 μm^2 with 256 × 256 pixels. During the sputtering cycle, the primary ion beam was operated in continuous (dc) mode and scanned across an area of 339 × 339 μm^2 for 2 s.

To collect the full data set containing the information on the emitted ions, neutrals and residual gas particles, each acquisition cycle consisted of three collected spectra with 40 000 repetitions (reps) each. First, the LPI spectrum was collected by firing the primary ion pulse and the laser. In the next spectrum, only the (positive) SIMS data was collected by only firing the ion pulse but blocking the laser beam. In the last acquisition cycle, the laser was fired into the vacuum chamber and the ion beam was blanked so as to only collect the residual gas spectrum. Since our instrument does not allow a fast automated switching of the detected ion polarity, negative SIMS depth profiles were acquired in separate experiments, where only the SIMS spectrum was collected in a data acquisition cycle. As a result, some experimental parameters such as the primary ion current and the ion detection efficiency may vary between the +SIMS/LPI and −SIMS profiles.

Wedge Crater. In addition to the depth profiling routine described above, a wedged crater[20] was created and analyzed. For that purpose, an area of 113 × 113 μm^2 was bombarded with a linearly increasing primary ion fluence along the *x*-direction of the eroded area through all four layers to the silicon substrate. The wedge-shaped crater was analyzed afterwards by collecting an image with a field of view of 226 × 226 μm^2 and 128 × 128 pixels. By analyzing the mass resolved information on each pixel, the positions of the interfaces between the different layers were determined with the aid of atomic force microscope (AFM) measurements.

AFM. To measure the dimension (width and depth) of the eroded wedge shaped crater, an atomic force microscope (AFM) (KLA Tencor, Nanopics 2100) was used and operated in contact mode. An area of 400 × 400 μm^2 was analyzed to fully include the crater and pristine surface region. After the measurement the pristine area was used to correct for the curvature in the measured data caused by bending of the piezo crystal and establish a zero value for the depth scale. To measure the dimensions of the crater, line scans were taken both parallel and perpendicular to the wedge direction as indicated in Figure S 1.

RESULTS AND DISCUSSION

This section is organized as follows. First, we show data taken on single component films of Irganox 1098 and Irganox 1010 in order to demonstrate the capability of laser post-ionization depth profiling and elucidate similarities and differences between molecular secondary ion and neutral analysis. We then switch to depth profiles obtained on the Irganox multilayer sample and investigate particularly the quantification of the measured molecular ion intensities in terms of the true sample composition.

Single Component Films. Examples of mass spectra obtained at the fresh surface of an Irganox 1010 film and after irradiation with a fluence of about 10^{13} ions/cm^2 are shown in Figure 2. The spectra labeled "SNMS" contain both the LPI

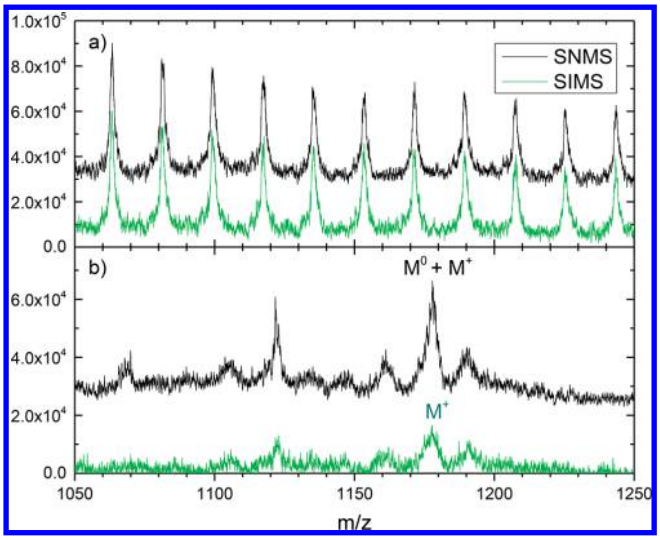

Figure 2. SIMS (lower trace) and SNMS (upper trace) spectra measured on (a) a fresh surface of an Irganox 1010 film covered with a thin water ice layer and (b) after irradiation of the film with 10^{13} ions/cm^2 under bombardment with 40 keV C_{60}^+ ions. For better illustration, the spectra have been vertically shifted against each other.

signal of postionized sputtered neutral particles as well as the secondary ion background, whereas those labeled "SIMS" depict the secondary ion spectrum alone. Both spectra were acquired under identical instrument conditions with the exception that the low mass signal was suppressed below *m/z* 200 during the SNMS measurement as explained in the Experimental Section. Before irradiation, both spectra mainly exhibit a series of water cluster peaks that originate from a thin ice overlayer that had been deposited on the cold surface prior to the analysis. These signals disappear after brief irradiation, exposing the molecular film to the analysis. From Figure 2b, it is obvious that meaningful LPI signals can be obtained for the molecular ion group around *m/z* 1176, which may contain contributions of the molecular ion M^+ of Irganox 1010 as well as the protonated or deprotonated molecules $[M + H]^+$, $[M + H_2]^+$, $[M - H]^+$, or $[M - H_2]^+$, which are not resolved here.

Throughout the remainder of this paper, we will therefore refer to this peak group as the M^0 signal for postionized neutrals and M+ or M^- signals for positive and negative secondary ions, respectively, with M representing the intact parent molecule of the investigated sample. It is interesting to note that the M^0 signal derived from the difference between both displayed spectra is at least as or even more intense than the corresponding M^+ signal observed in the SIMS spectrum. This finding indicates a rather efficient post-ionization mechanism, because the focused laser is known to sample only a small fraction (typically or the order of 10^{-2}) of the sputtered material.[21]

In order to examine the prospects of molecular SIMS/SNMS depth profiling, sputter depth profiles obtained on this system are shown in Figure 3, where the M^0 (LPI) and M^+ (SIMS) signals are followed as a function of the applied primary ion fluence. The LPI profile was obtained by subtracting the SIMS background and therefore directly represents the postionized

DOI: 10.1021/acs.jpcc.7b02596
J. Phys. Chem. C 2017, 121, 19705−19715

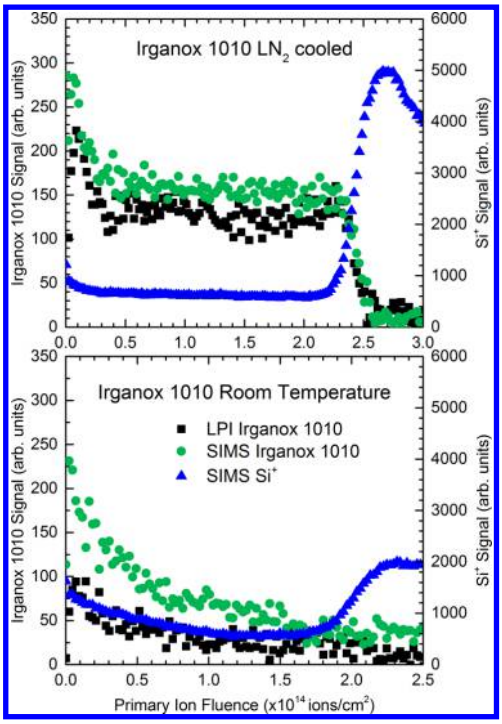

Figure 3. SIMS (M^+) and LPI (M^0) depth profiles obtained on a 100 nm Irganox 1010 film on silicon under bombardment with 40 keV C_{60}^+ ions.

sputtered neutral molecules. For comparison, depth profiles taken at room temperature are displayed along with those taken with the sample stage held at liquid nitrogen temperature, confirming that meaningful depth profiles can on this system only be obtained under low temperature conditions as observed earlier.[22−24] Both the LPI and SIMS profiles exhibit essentially the same features, namely an initial increase of the signal as the ice overlayer is removed, followed by an exponential decay into a steady state as explained by the erosion dynamics model.[25,26] The ratio between the secondary ion and neutral signal decreases with increasing ion fluence, starting at about 2 at the surface and reaching a constant value of about 1.2 in the steady state. This finding indicates that the presence of the ice overlayer increases the ionization probability, presumably via protonation of sputtered Irganox molecules. The fluctuations observed in the steady state are mostly due to statistical noise, which for the case of LPI are superimposed by additional fluctuations caused by small temporal variations of the post-ionization laser intensity. Apart from these fluctuations, it is seen that the molecular ion intensity remains constant in both modes, until at a fluence of about 2.4 ions/nm^2 the interface to the underlying silicon substrate is reached. In order to confirm that the film was completely eroded, the Si^+ secondary ion signal is plotted as well. The fact that the 50% intensity of both the LPI and SIMS molecular ion signal are reached at the same fluence where the substrate signal has risen to half its maximum value confirms that there is no interlayer between the Irganox film and the silicon substrate.

Multilayer Sample. In the following discussion of data obtained on the Irganox multilayer system, we will refer to the sample constituents Irganox 1098 and Irganox 1010 simply as "1098" and "1010", respectively. SIMS depth profiles of the multilayer sample obtained in positive and negative secondary ion mode are shown in Figure 4. In both modes, all four layers of the system can be unambiguously identified.

The number of sputter cycles needed to reach the interfaces between the different layers and to the underlying silicon substrate slightly varies between both profiles shown in Figure 4, because the positive and negative ion profiles were obtained in separate experiments where the C_{60}^+ primary ion current was not exactly the same. In fact, the data show that the ion current used in the negative SIMS profile was about 25% higher than that used in the positive SIMS/SNMS profile, an information that will be useful for the depth scale calibration as well as the calculation of ionization probabilities as described below. The negative ion spectrum shows the expected behavior with the 1098 signal being visible in the 1098 containing layers 1, 2, and 3 and the 1010 signal visible in the 1010 containing layers 2 and 4. Moreover, both the 1098 and the 1010 signals are smaller in the intermixed layer 2 than in the respective pure layers, thereby qualitatively reflecting the smaller concentration (or volume fraction) of both constituents within this layer. On the other hand, the positive ion spectrum deviates from the

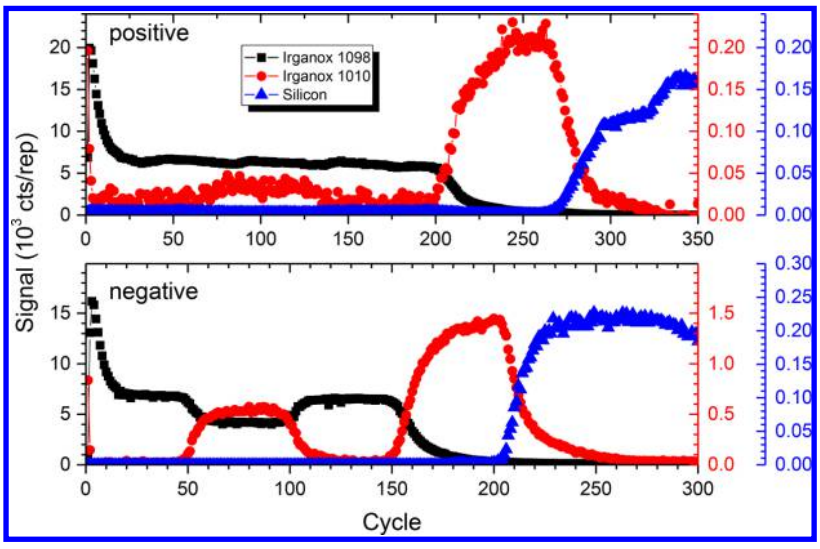

Figure 4. Depth profile of positive and negative molecule specific secondary ion signals M^+ and M^- obtained on the Irganox 1098/1010 multilayer sample under bombardment with 40 keV C_{60}^+ ions.

DOI: 10.1021/acs.jpcc.7b02596
J. Phys. Chem. C 2017, 121, 19705−19715

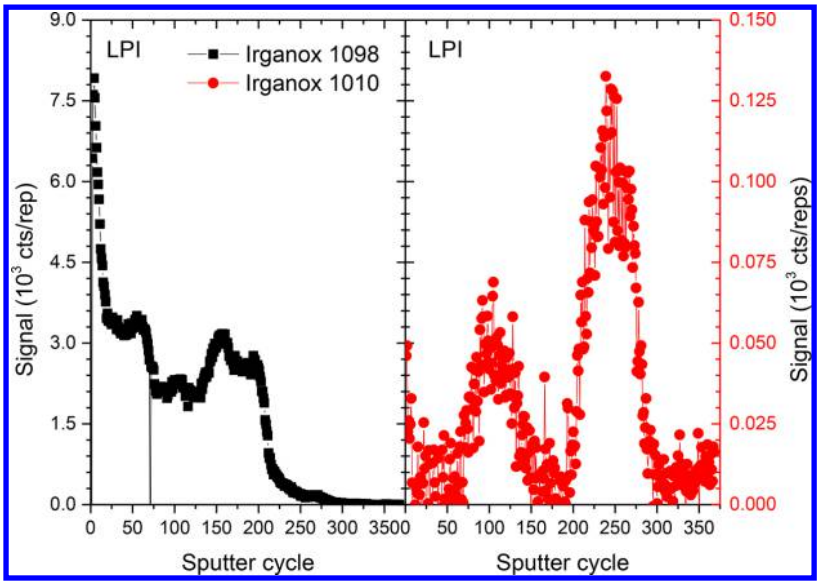

Figure 5. Depth profile of postionized neutral molecule signal M^0 obtained on the Irganox 1098/1010 multilayer sample under bombardment with 40 keV C_{60}^+ ions.

expected behavior insofar as the 1098 signal does not decrease in the intermixed layer. This observation already qualitatively shows that there must be a pronounced matrix effect in the sense that the formation probability of the M_{1098}^+ ion group must be significantly enhanced by the presence of 1010. A depth profile of the corresponding postionized neutral molecules, which was acquired simultaneously with the positive SIMS profile in Figure 4, is shown in Figure 5. Qualitatively, the data show the expected signal trends in the same way as observed in the negative secondary ion profile. The fact that the signal-to-noise ratio in the LPI depth profiles appears to be worse than that in the corresponding SIMS profiles is caused by long-term fluctuations of the post-ionization laser intensity. As will be shown below, the influence of these fluctuations largely cancels when the profiles are quantified.

Signal Quantitation. In order to arrive at a more quantitative characterization of matrix effects, we examine the quantitation of the measured depth profiles. In principle, the secondary ion intensity measured for a sputtered species X is given as

$$S_X^{\pm} = I_p \cdot Y_X \cdot \alpha_X^{\pm} \cdot \eta_X^{\pm} \tag{1}$$

where I_p denotes the primary ion flux, Y_X denotes the partial sputter yield, that is, the average number of emitted species X per projectile ion impact, $\alpha_X^{\pm}$ is the ionization probability, that is, the probability that a sputtered species X is emitted as a positive or negative secondary ion. The quantity $\eta_X^{\pm}$ is a transmission factor, which for the case of a pulsed ToF experiment has the dimension of time and essentially describes the fraction of emitted secondary ions that are sampled by the instrument. For the postionized neutral signal, an equivalent relation holds as

$$S_X^0 = I_p \cdot Y_X \cdot (1 - \alpha_X^{\pm}) \alpha_X^0 \cdot \eta_X^0 \tag{2}$$

where α_X^0 describes the post-ionization probability for a sputtered neutral species X. In an LPI experiment, the factor η_X^0 is a complicated function of the geometric overlap between the laser beam and the plume of sputtered particles as well as the timing of the laser pulse with respect to the primary ion pulse.[14] It remains constant and independent of the sample composition if the emission velocity and angle distributions of the detected neutral particles do not significantly change.

In many cases, the majority of the sputtered material is emitted as neutrals, and the values of $\alpha_X^{\pm}$ are small. In that case, the measured post-ionization signal is proportional to the partial sputter yield, which under steady state sputtering conditions must reflect the sample stoichiometry as

$$Y_X = c_X \cdot Y_{tot} \tag{3}$$

where Y_{tot} denotes the total sputter yield. For a molecular signal, an additional fragmentation factor must be introduced into eq 3, which may either describe the survival of an intact molecule or the formation of a specific fragment during the emission process. For the present discussion, we assume this factor to be independent of the film stoichiometry, so that the post-ionization signal measured for the molecular ion of component i (1098 or 1010) should to first order be given as

$$S_i^0(c_i) \propto c_i \cdot Y_{tot} \tag{4}$$

The corresponding secondary ion signal, on the other hand, is described by

$$S_i^{\pm}(c_i) \propto c_i \cdot Y_{tot} \cdot \alpha_i^{\pm} \tag{5}$$

where the quantity $\alpha_i^{\pm}$ now describes the effective ionization probability of an ejected intact Irganox molecule, for instance, by protonation or deprotonation. It is this quantity that may critically depend on the sample composition and therefore describes the matrix effect. We wish to emphasize that all measured signals are proportional to the total sputter yield, which may also depend on the surface composition and change between different layers. Even in the absence of ionization matrix effects, a measured mass spectrometric signal representing a component i therefore is not necessarily proportional to its concentration.

A relatively straightforward way to investigate for possible sputter yield changes as a function of concentration is to look for signal correlation, for instance, at the interfaces in the depth profiles of a multilayer system. For the two-component system investigated here, this is simply done by plotting the 1010

DOI: 10.1021/acs.jpcc.7b02596
J. Phys. Chem. C 2017, 121, 19705−19715

signal against the 1098 signal in the depth profiles of Figures 3 and 4. The resulting correlation plots are shown in Figure 6. It

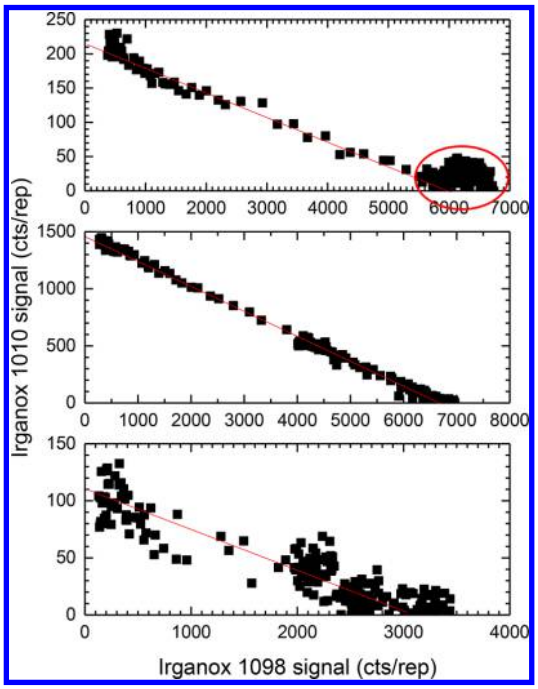

Figure 6. Correlation between molecule specific secondary ion (M^+ and M^-) and postionized neutral (M^0) signals of Irganox 1010 versus Irganox 1098. The indicated lines represent linear fits to the data as described in the text. The circle indicates the data points that were collected while profiling through the pure 1098 layers and the intermixed layer as discussed in the text.

is clear that the assumption of a constant fragmentation probability underlying eqs 4 and 5 is violated at the start of the depth profile, where the signals decay into the steady state, and therefore these points were excluded from the plots. Moreover, the assumption of a two component system is violated as soon as the silicon substrate signal begins to rise, so that the data points after the maximum of the 1010 signal in layer 4 were also excluded.

Interestingly, a linear correlation is observed in all three profiles, indicating that there is no significant change of the sputter yield across the interfaces between the different layers. While the linear correlation is expected for the post-ionization experiment, it is surprising to see for the SIMS depth profiles because in this case a linear correlation is only rigorously expected if the ionization probability $\alpha_i^{\pm}$ is constant across the interface. At least for the positive ion spectrum, however, it is clear that there must be a rather significant matrix effect. A close inspection of the data reveals that the straight line drawn in the upper panel of Figure 6 is somewhat misleading, because all of the data points collected while profiling through the pure 1098 layers and the intermixed layer, which span a concentration interval between 0.5 and 1, fall into the circled area. The observed quasi-linear dependence indicated by the straight line therefore only holds for the interface between the pure 1098 layer 3 and the pure 1010 layer 4. Obviously, a nonlinear concentration dependence of one signal may be coincidentally compensated by a nonlinearity in another signal, leading to an apparently linear correlation as well.

The relatively large scatter of the post-ionization data shown in the correlation plot of Figure 6 is disturbing, but it has to be kept in mind that both signals vary as a result of varying laser intensity. These variations, as well as possible variations of the primary ion current, can be eliminated from the quantitation by normalizing the measured signals to the weighted signal sum. Assuming a constant relative sensitivity for all constituents in the system, the concentration of a component i can be obtained at all points of the depth profile via

$$c_i = \frac{I_i}{\sum_j I_j} \text{ with } I_j = S_j \cdot \mathrm{RSF}_j^i \tag{6}$$

where the relative sensitivity factor RSF_j^i can be obtained from a standard material of known composition. For the system studied here, we determine these values from the signals measured for the pure 1098 and 1010 layers and the silicon substrate, respectively. The resulting concentration profile determined from the positive SIMS profile is shown in Figure 7.

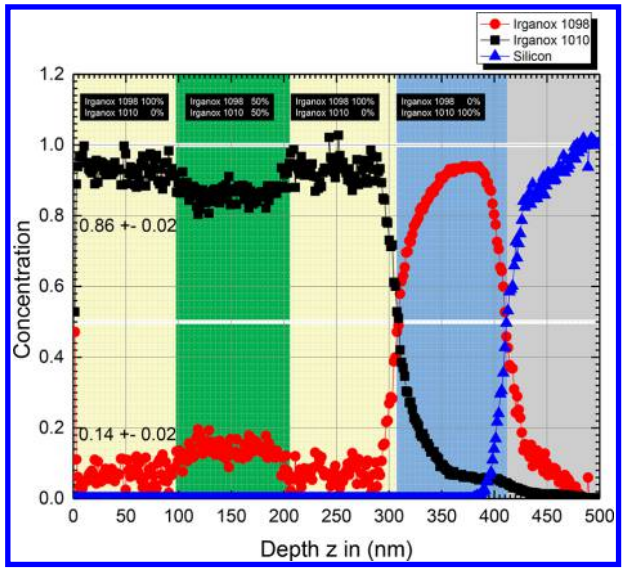

Figure 7. Quantitation of positive SIMS depth profile under assumption of constant relative sensitivity factors between Irganox 1098, Irganox 1010, and silicon substrate signals.

It is seen that the assumption of a constant RSF must clearly be wrong, because the calculated concentrations in layer 2, as indicated in the figure, deviate from the known true stoichiometry of this layer. We can take the deviation of these values from the expected result of 0.5 as a measure of the observed matrix effect. Alternatively, we can adopt the definition of the matrix effect magnitude[8,9]

$$\Xi_i = 2 \int_0^1 \frac{S_i(c_i)}{S_1^i} \, \mathrm{d}c_i - 1 \tag{7}$$

and approximate the integral by a polygon between $c_i = 0$, 0.5, and 1. In eq 7, S_1^i denotes the signal measured for a pure layer of component i. A value of $\Xi = 0$ indicates ideal (matrix effect free) behavior, whereas $\Xi < 0$ indicates suppression and $\Xi < 0$ indicates enhancement of the secondary ion formation for component i. In principle, the value of Ξ_i, as defined by eq 7, can vary between −1 and 1 but our crude approximation using only the signals measured at c = 50% and c = 100% only permits a maximum possible absolute value of 0.5. For the positive secondary ions, the resulting $\Xi_{1098} = +0.5$ and $\Xi_{1010} = -0.35$ obviously describe a rather severe matrix effect, where

DOI: 10.1021/acs.jpcc.7b02596
J. Phys. Chem. C 2017, 121, 19705−19715

the 1098 signal is strongly enhanced by the presence of 1010 signal and the 1010 signal is strongly suppressed by the presence of 1098.

The situation changes if the negative ion profile is analyzed. Using the same quantitation procedure, we find the concentration plot shown in Figure 8. It is evident that the

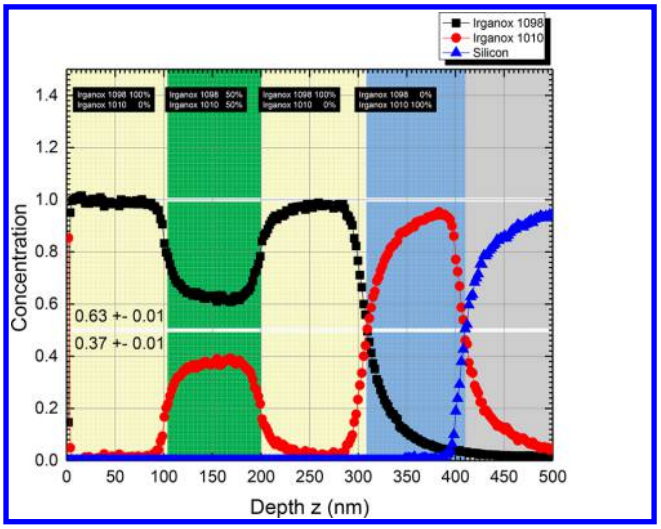

Figure 8. Quantitation of negative SIMS depth profile under assumption of constant relative sensitivity factors between Irganox 1098, Irganox 1010, and silicon substrate signals.

true composition of the intermixed layer is much better represented by the M^- signals, yielding a concentration of c_{1098} = 0.63 in this layer. There is, however, a remaining matrix effect enhancing the 1098 signal with Ξ_{1098} = +0.21, whereas Ξ_{1010} = −0.04 indicates an almost ideal behavior of the 1010 signal.

The concentration profile derived from the secondary neutral profile is depicted in Figure 9. It is evident that the LPI experiment provides the closest representation of the true stoichiometry within the intermixed layer, yielding a 1098 concentration value of 0.57. The corresponding values of the

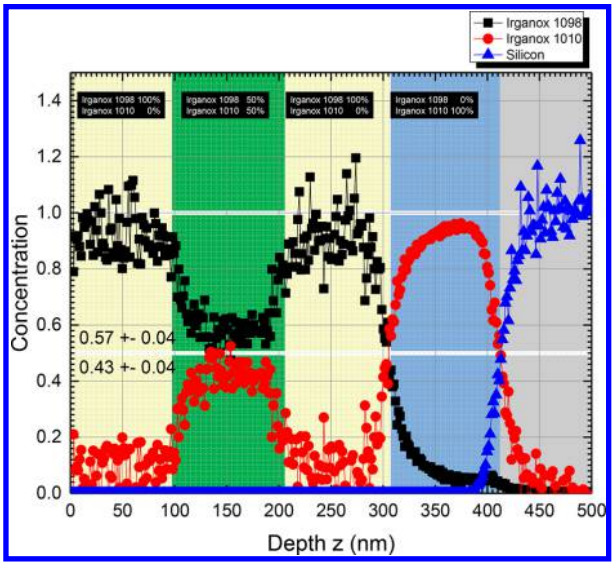

Figure 9. Quantitation of SNMS depth profile under assumption of constant relative sensitivity factors between Irganox 1098, Irganox 1010, and silicon substrate signals.

remaining matrix effect magnitude are Ξ_{1098} = −0.14 and Ξ_{1010} = +0.05. In other words, the 1098 signal appears to be slightly suppressed by the presence of 1010, whereas the 1010 signal again exhibits nearly ideal behavior. In principle, ionization matrix effects should avoided in post-ionization experiments, and influences of the SIMS ionization matrix effect upon the post-ionization data are expected to be negligible because the absolute value of the SIMS ionization probability is small ($\sim 10^{-3}$).[6,7] Therefore, the suppression observed for the 1098 M^0 signal must be caused by a matrix dependent variation in the emission angle and/or energy distribution of the sputtered neutral molecules. Similar effects were observed recently by Karras and Lockyer,[27] who found a drastic suppression effect in a two component drug mixture when analyzed at low temperature, which was not found at room temperature. Also in this case, the observed suppression effect was attributed to a temperature-dependent change in the sputtering characteristics of the neutral molecules. It should be noted, however, that such variations would likely influence the SIMS data in the same way. The fact that *enhancement* is observed for the 1098 M^- signal therefore indicates that the ionization matrix effect observed in the negative SIMS profile must be even greater than indicated by the SIMS data alone. Another possible cause for a matrix effect in post-ionization spectra would be a matrix-dependent change in the excitation state of the ejected molecules, which could in principle influence the effective post-ionization efficiency via changes in the laser-induced-photoionization and -fragmentation probability. A detailed analysis of the depth profiling behavior observed for different fragment signals would probably provide more inside here but is outside the scope of the present paper.

Depth Axis Calibration. Apart from the composition calibration, an important point regarding the quantitation of a sputter depth profile concerns the conversion of applied primary ion fluence into eroded depth. This is of particular interest for a multilayer system, because the sputter yield and, hence, the erosion rate may in principle change between different layers of the sample. In order to examine this for the system studied here, we eroded a wedge-shaped crater into the film by applying a linearly increasing ion fluence between opposite sides of the raster area. As described in detail elsewhere,[23,24] this strategy allows the detection of variations of the erosion rate by means of a profilometric characterization of the resulting crater, where depth-dependent variations of the erosion rate translate into a varying slope of the crater bottom. An AFM image of the eroded crater is shown in the Supporting Information Figure S1. A line scan along the wedge direction, as indicated in the AFM image, is shown in Figure 10 (upper panel). Apart from a small disturbance at the very surface, which may either be induced by an artifact of the AFM analysis or by redeposition of sputtered material, it is seen that the crater bottom exhibits a constant slope until at a depth of about 410 nm the silicon substrate is reached.

At this point, the slope abruptly changes to a smaller value, reflecting the fact that the C_{60} beam erodes silicon with a much slower rate than the organic film.

In order to unambiguously identify the different layers, a SIMS image of the crater was acquired in negative ion mode. Applying the quantitation according to eq 6 to the relevant ion signals of a line scan along the same direction as the AFM scan, we find the result depicted in the lower panel of Figure 10, showing that the position of the different layers as well as the interfaces between them can be clearly discerned, thereby

DOI: 10.1021/acs.jpcc.7b02596
J. Phys. Chem. C 2017, 121, 19705−19715

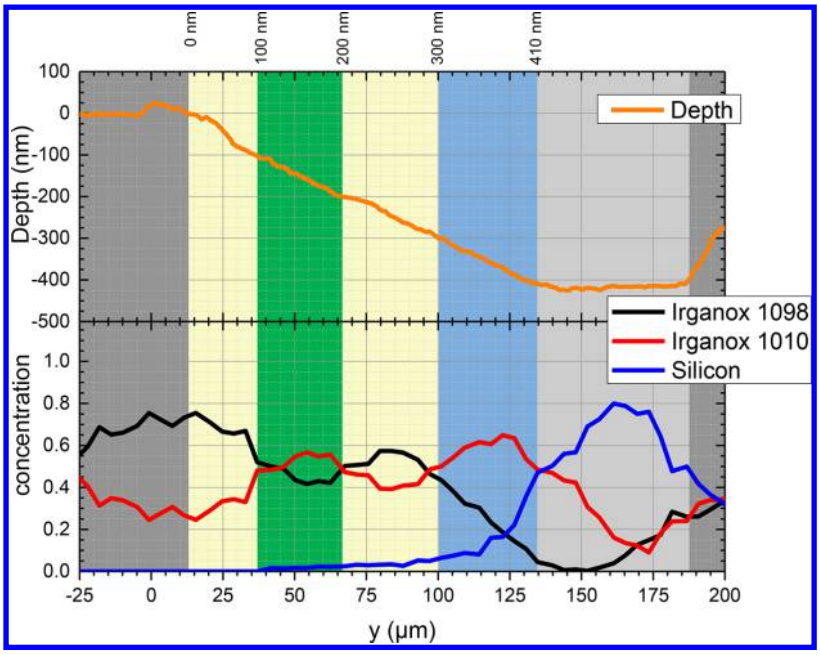

Figure 10. Upper panel: AFM line scan across a wedge crater eroded into the Irganox multilayer sample using a 40 keV C_{60}^+ ion beam. Bottom panel: line scan data across a negative secondary ion image of the wedge crater. The concentration was calculated according to eq 6 as described in the text.

allowing the examination of the thickness of the individual layers. The results are presented in Table 1 and show that the erosion rate remains constant at a value of about 2 nm/cycle within experimental error throughout the removal of the entire film.

Table 1. Relative Erosion Rates and Individual Layer Thicknesses within the Irganox 1098/1010 Multilayer System As Determined from the Data in Figure 10

	layer thickness (nm)	relative erosion rate (nm/cycle)
Layer 1	100	1.9
Layer 2	100	2.0
Layer 3	100	1.8
Layer 4	121	2.3

As a consequence, we can linearly convert the applied ion fluence (or sputter cycle number) to eroded depth by assigning the point where the evaluated silicon substrate concentration reaches 50% to the total eroded depth of about 410 nm. This procedure forms the basis of the depth axis calibration provided in Figures 7–9.

Ionization Efficiency. Using the concentration data determined from the sputtered neutral depth profile, the core information describing the matrix effect, that is, the variation of the ionization efficiency for a sputtered molecule as a function of the sample composition, may be extracted. The interface region between the different Irganox layers is of special interest. For the binary 1098/1010 system studied here, the interfaces between layers 1, 2, 3, and 4 will in the following be referred to as interface 1 (layer 1–layer 2), 2 (layer 2–layer 3) and 3 (layer 3–layer 4), respectively. According to eqs 4 and 5, the positive ionization efficiency is directly calculated from the data in Figures 4 and 5 by dividing the positive SIMS signal by the corresponding LPI signal measured at each cycle. For the negative ions, the situation is more complicated because the SIMS and LPI depth profiles were measured in two separate experiments. Therefore, the depth scales are not exactly the same and the data have to be interpolated in order to calculate the negative ionization probability. In order to reduce the statistical noise, the raw data traces shown in Figures 4 and 5 were smoothed using a 16 point Savitzky-Golay algorithm prior to the division. Because the proportionality factors in eqs 4 and 5 can be assumed to be independent of the sample composition at least to first order, the ion/neutral signal ratio represents the relative variation of the ionization probability as a function of the applied ion fluence, which can then be compared to the sample stoichiometry calculated at this depth. The result is plotted for both the M^+ and M^- ion groups of Irganox 1098 and Irganox 1010 in Figure 11.

The first and probably most import observation is that there is no unique correlation between the sample stoichiometry and the ionization efficiency. In order to unravel the reason for the apparent scatter, the data points have been marked by different symbols depending upon the interface region they were extracted from. While the full symbols refer to the interface 3 between the pure 1098 and 1010 films, the open symbols characterize the interfaces 1 and 2 between the intermixed layer 2 and a pure 1098 layer. It is obvious that even if the same average concentration (or volume fraction) is measured while going through different interfaces, there must be distinct differences in the sample chemistry determining the ionization efficiency of a sputtered molecule.

For positive ionization, interface 3 between the two pure films (closed symbols) is characterized by an almost constant ionization efficiency for the 1098 molecule within the range $0 \leq c_{1010} \leq 0.5$, while that of the 1010 molecule goes through a distinct minimum around $c_{1010} \approx 0.2$. Toward large 1010 content, both values are found to slightly increase, until at $c_{1010} > 0.9$ the ionization probability of the 1098 molecule suddenly increases. The latter finding may either be real and indicate an efficient deprotonation of the Irganox 1098 molecule if diluted in an almost pure 1010 matrix, or the apparent increase is caused by a problem regarding the background subtraction of

DOI: 10.1021/acs.jpcc.7b02596
J. Phys. Chem. C 2017, 121, 19705–19715

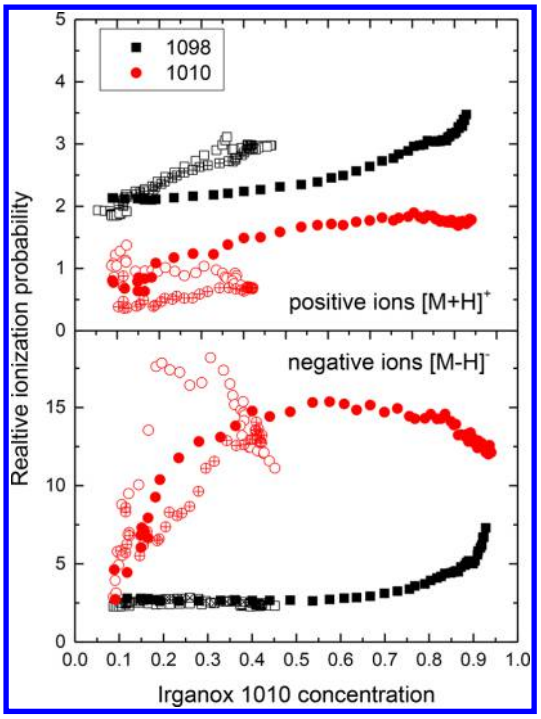

Figure 11. Relative positive (upper panel) or negative (lower panel) ionization probability of sputtered Irganox 1098 and 1010 molecules versus surface composition monitored by Irganox 1010 concentration. Closed symbols: data derived from the interface between layer 3 and 4; open symbols: data derived from the interfaces between layer 1 and 2 (square, circle) and between layer 2 and 3 (square with lines, circle with lines).

the 1098 post-ionization signal that is very low in that region. On the other hand, the interfaces to the intermixed film (open symbols), reveal a pronounced increase of the 1098 ionization efficiency as soon as the 1010 concentration exceeds about 10%. Interestingly, α^{+}_{1098} exhibits a similar dependence for both interfaces, whereas α^{+}_{1010} behaves qualitatively different.

For negative ions, the ionization probability of 1098 appears to be largely independent of the 1010 concentration. On the other hand, the negative ionization efficiency for the 1010 molecule, depends strongly on the sample composition in the range $0 \leq c_{1010} \leq 0.5$, indicating a rather strong matrix effect for these ions. The apparent structure observed in this concentration range might at least partly be due to an uncertainty regarding the matching of the interfaces, because SIMS and SNMS spectra were taken in different depth profiles as explained above. Above a 1010 content of 50%, however, both ionization probabilities remain constant over a relatively wide concentration range. We believe that this is the reason for the apparently good quantitation result obtained for the intermixed layer with $c_{1010} = 0.5$. At low 1010 concentration, our data indicate a strong increase of its ionization efficiency by three-fold between $c_{1010} = 0.1$ and 0.5. In particular, for the first interface the negative ionization probability of the Irganox 1010 molecule appears to go through a pronounced maximum, whereas an almost linear increase is found for the other two interfaces. Because both interfaces 1 and 2 characterize the transition between the intermixed layer and a pure 1098 film, we are forced to conclude that the surface chemistry leading to the formation of the negatively ionized sputtered Irganox 1098 molecules must be different in both cases.

These findings are remarkable because they appear to contradict the results presented in the VAMAS round robin study[9] performed on an Irganox 1098/1010 multilayer sample similar to that investigated here, where only rather weak matrix effects were found even for the quasi-molecular ions of that system. One has to keep in mind, however, that nearly all of the experiments participating in the VAMAS study were performed using an Ar_n^+ cluster ion beam for depth profiling and a Bi_n^+ cluster ion beam for data acquisition with the exception of three experiments where the Ar_n^+ sputtering beam was used in order to generate the mass spectral data as well. On the other hand, the data presented here were acquired using a C_{60}^+ ion beam for depth profiling and data acquisition. It has been shown that the surface chemistry induced by C_{60} impact might strongly deviate from that generated by small metal clusters, thereby in some cases strongly promoting the positive ionization efficiency of sputtered molecules.[28]

At the present time, we can only speculate about the reason for the observed variations of the ionization efficiency. In principle, both the protonation and deprotonation of a sputtered molecule must be triggered by ion impact-induced fragmentation reactions. From the magnitude difference between the observed SIMS and LPI signals of 1010 and 1098, it is clear that the larger 1010 molecule must experience significantly stronger fragmentation than the smaller 1098 molecule. From this perspective, it appears reasonable that ionization efficiencies may be enhanced by a larger 1010 content. During the transition between two pure and homogeneous films, both materials are single phase and the interface chemistry is solely governed by ion bombardment induced mixing. On the other hand, the intermixed layer of the sample studied here was manufactured by alternating deposition of thin 1098 and 1010 films. The microstructure of the resulting film is not clear, but it is reasonable to doubt that the resulting film is completely homogeneous. Therefore, the signal produced by ions impacting on different surface areas may be strongly different, even though the average volume fraction probed by the SIMS/SNMS experiment is the same, thereby accounting for the different behavior at different interfaces. Moreover, the 1098 signal variations observed at interface 1 originate from upward mixing of 1010 into the depth interval probed by the sputtering process from below, whereas the variations in interface 2 are caused by downward mixing of an enhanced 1010 content out of the probed depth interval. It is a well-known fact in inorganic SIMS that both mixing processes might be vastly different, leading, for instance, to different upward and downward slopes of the signal when depth profiling through a delta layer,[29−31] The role of these mixing processes in connection with sample topology and composition with respect to the chemical ionization process is yet unclear, and further work is needed to completely understand the ion-induced surface chemistry governing the protonation and deprotonation process of sputtered molecules.

CONCLUSIONS

The work presented in this study shows that successful depth profiles of organic molecules as complex and heavy as Irganox 1098 and Irganox 1010 cannot only be collected for secondary ions but also for the postionized neutral species. Strong field ionization is capable of providing molecular information through the entirety of the depth profile if the sample is cooled via liquid nitrogen. The detection of both secondary ions and postionized secondary neutral species leads to a signal

DOI: 10.1021/acs.jpcc.7b02596
J. Phys. Chem. C 2017, 121, 19705−19715

enhancement of a factor of 2 through the depth profile while only sampling a small fraction of the plume of sputtered neutral material. There is, however, significant headroom for further improvement if a more intense post-ionization laser was used that could then be defocused to irradiate the entire detectable plume of sputtered neutral particles with comparable intensity.

The data presented here demonstrate the capability of laser post-ionization to strongly reduce and almost completely overcome matrix ionization effects by decoupling the sputtering and ionization processes. Without post-ionization, single beam C_{60} depth profiling was neither in positive nor in negative mode capable of revealing the stoichiometric composition of the sample system. Although the results measured in negative mode deviate by 24% from the composition of the sample, the results collected in positive mode show a difference of 68% from the real concentration due to more pronounced matrix ionization effects. Moreover, one should note that matrix effects observed in molecular SIMS clearly depend on the projectile used to generate the mass spectral data, whereas this projectile dependence can be expected to be much less pronounced for the sputtered neutral molecules.

■ ASSOCIATED CONTENT

Supporting Information

The Supporting Information is available free of charge on the ACS Publications website at DOI: 10.1021/acs.jpcc.7b02596.

AFM image of wedge-shaped crater (PDF)

■ AUTHOR INFORMATION

Corresponding Author

*E-mail: Lars.breuer@psu.edu.

ORCID

Lars Breuer: 0000-0002-7797-9662

Notes

The authors declare no competing financial interest.

■ ACKNOWLEDGMENTS

This project was financially supported by the National Institutes of Health (Grant 5R01GM113746-22).

■ REFERENCES

(1) Winograd, N. The Magic of Cluster Sims. *Anal. Chem.* **2005**, *77*, 142A−149A.

(2) Gillen, G.; Simons, D. S.; Williams, P. Molecular Ion Imaging and Dynamic Secondary-Ion Mass Spectrometry of Organic Compounds. *Anal. Chem.* **1990**, *62*, 2122−2130.

(3) Wucher, A.; Fisher, G. L.; Mahoney, C. M. Three-Dimensional Imaging with Cluster Ion Beams. In *Cluster Secondary Ion Mass Spectrometry*; John Wiley & Sons, Inc., 2013; pp 207−246.

(4) Mahoney, C. M.; Wucher, A. Molecular Depth Profiling with Cluster Ion Beams. In *Cluster Secondary Ion Mass Spectrometry*; John Wiley & Sons, Inc., 2013; pp 117−205.

(5) Shard, A. G.; Gilmore, I. S.; Wucher, A. Molecular Depth Profiling. In *Tof-Sims: Materials Analysis by Mass Spectrometry*; IM Publications and SurfaceSpectra: Chichester, 2013; pp 311−334.

(6) Popczun, N. J.; Breuer, L.; Wucher, A.; Winograd, N. On the SIMS Ionization Probability of Organic Molecules. *Surf. Interface Anal.* **2017**, 1−10.

(7) Popczun, N.; Breuer, L.; Wucher, A.; Winograd, N. Ionization Probability in Molecular SIMS: Protonation Efficiency of Sputtered Guanine Molecules Studied by Laser Post-Ionization. *J. Phys. Chem. C* **2017**, *121*, 8931.

(8) Shard, A. G.; Spencer, S. J.; Smith, S. A.; Havelund, R.; Gilmore, I. S. The Matrix Effect in Organic Secondary Ion Mass Spectrometry. *Int. J. Mass Spectrom.* **2015**, *377*, 599−609.

(9) Shard, A. G.; Havelund, R.; Spencer, S. J.; Gilmore, I. S.; Alexander, M. R.; Angerer, T. B.; Aoyagi, S.; Barnes, J.-P.; Benayad, A.; Bernasik, A.; et al. Measuring Compositions in Organic Depth Profiling: Results from a Vamas Interlaboratory Study. *J. Phys. Chem. B* **2015**, *119*, 10784−10797.

(10) Sheraz née Rabbani, S.; Barber, A.; Berrueta Razo, I.; Fletcher, J. S.; Lockyer, N. P.; Vickerman, J. C. Prospect of Increasing Secondary Ion Yields in Tof-SIMS Using Water Cluster Primary Ion Beams. *Surf. Interface Anal.* **2014**, *46*, 51−53.

(11) Sheraz née Rabbani, S.; Razo, I. B.; Kohn, T.; Lockyer, N. P.; Vickerman, J. C. Enhancing Ion Yields in Time-of-Flight-Secondary Ion Mass Spectrometry: A Comparative Study of Argon and Water Cluster Primary Beams. *Anal. Chem.* **2015**, *87*, 2367−2374.

(12) Wucher, A.; Tian, H.; Winograd, N. A Mixed Cluster Ion Beam to Enhance the Ionization Efficiency in Molecular Secondary Ion Mass Spectrometry. *Rapid Commun. Mass Spectrom.* **2014**, *28*, 396−400.

(13) Tian, H.; Wucher, A.; Winograd, N. Reducing the Matrix Effect in Organic Cluster Sims Using Dynamic Reactive Ionization. *J. Am. Soc. Mass Spectrom.* **2016**, *27*, 2014−2024.

(14) Wucher, A. Laser Postionization - Fundamentals. In *Tof-Sims: Materials Analysis by Mass Spectrometry*; 2nd ed.; Vickerman, J. C., Briggs, D., Eds.; IM Publications and SurfaceSpectra, 2013; pp 217−246.

(15) Kucher, A.; Jackson, L. M.; Lerach, J. O.; Bloom, A. N.; Popczun, N. J.; Wucher, A.; Winograd, N. Near Infrared (Nir) Strong Field Ionization and Imaging of C-60 Sputtered Molecules: Overcoming Matrix Effects and Improving Sensitivity. *Anal. Chem.* **2014**, *86*, 8613−8620.

(16) Willingham, D.; Kucher, A.; Winograd, N. Strong-Field Ionization of Sputtered Molecules for Biomolecular Imaging. *Chem. Phys. Lett.* **2009**, *468*, 264−269.

(17) Braun, R. M.; Mullock, S. J.; Corlett, C.; Willey, K. F.; Vickerman, J. C.; Winograd, N. Performance Characteristics of a Chemical Imaging Tof Mass Spectrometer. *Rapid Commun. in Mass Spec.* **1998**, *12*, 1246−1252.

(18) Willingham, D.; Kucher, A.; Winograd, N. Strong-Field Ionization of Sputtered Molecules for Biomolecular Imaging. *Chem. Phys. Lett.* **2009**, *468*, 264−269.

(19) Kucher, A.; Wucher, A.; Winograd, N. Strong Field Ionization of β-Estradiol in the Ir: Strategies to Optimize Molecular Postionization in Secondary Neutral Mass Spectrometry. *J. Phys. Chem. C* **2014**, *118*, 25534−25544.

(20) Mao, D.; Lu, C.; Winograd, N.; Wucher, A. Molecular Depth Profiling by Wedged Crater Beveling. *Anal. Chem.* **2011**, *83*, 6410−6417.

(21) Breuer, L.; Kucher, A.; Herder, M.; Wucher, A.; Winograd, N. Formation of Neutral In_nC_m Clusters under C60 Ion Bombardment of Indium. *J. Phys. Chem. A* **2014**, *118*, 8542.

(22) Sjovall, P.; Rading, D.; Ray, S.; Yang, L.; Shard, A. G. Sample Cooling or Rotation Improves C-60 Organic Depth Profiles of Multilayered Reference Samples: Results from a Vamas Interlaboratory Study. *J. Phys. Chem. B* **2010**, *114*, 769−774.

(23) Mao, D.; Lu, C.; Winograd, N.; Wucher, A. Molecular Depth Profiling by Wedged Crater Bevelling. *Anal. Chem.* **2011**, *83*, 6410−6417.

(24) Mao, D.; Wucher, A.; Winograd, N. Molecular Depth Profiling with Cluster Secondary Ion Mass Spectrometry and Wedges. *Anal. Chem.* **2010**, *82*, 57−60.

(25) Wucher, A. A Simple Erosion Dynamics Model for Molecular Sputter Depth Profiling. *Surf. Interface Anal.* **2008**, *40*, 1545−1551.

(26) Cheng, J.; Wucher, A.; Winograd, N. Molecular Depth Profiling with Cluster Ion Beams. *J. Phys. Chem. B* **2006**, *110*, 8329−8336.

(27) Karras, G.; Lockyer, N. P. Quantitative Surface Analysis of a Binary Drug Mixture-Suppression Effects in the Detection of Sputtered Ions and Post-Ionized Neutrals. *J. Am. Soc. Mass Spectrom.* **2014**, *25*, 832−840.

DOI: 10.1021/acs.jpcc.7b02596
J. Phys. Chem. C 2017, 121, 19705−19715

(28) Wucher, A. Molecular Secondary Ion Formation under Cluster Bombardment: A Fundamental Review. *Appl. Surf. Sci.* **2006**, *252*, 6482−6489.
(29) Dowsett, M. G.; Rowlands, G.; Allen, P. N.; Barlow, R. D. An Analytic Form for the SIMS Response Function Measured from Ultra-Thin Impurity Layers. *Surf. Interface Anal.* **1994**, *21*, 310−315.
(30) Hofmann, S. Ultimate Depth Resolution and Profile Reconstruction in Sputter Profiling with AES and SIMS. *Surf. Interface Anal.* **2000**, *30*, 228−236.
(31) Zalm, P. C.; de Kruif, R. C. M. Problems in the Deconvolution of SIMS Depth Profiles Using Delta-Doped Test Structures. *Appl. Surf. Sci.* **1993**, *70*−*71*, 73−78.

DOI: 10.1021/acs.jpcc.7b02596
J. Phys. Chem. C 2017, 121, 19705−19715